DEM analyses of impact induced rock fragmentation

Weigang Shen[1], Tao Zhao[1,2*], Giovanni Crosta[3], Feng Dai[1]

[1]State Key Laboratory of Hydraulics and Mountain River Engineering, College of Water Resource and Hydropower, Sichuan University, Chengdu, 610065, China

[2] Key Laboratory of Geotechnical and Underground Engineering (Tongji University), Ministry of Education, Shanghai, 200092, China

[3]Department of Earth and Environmental Sciences, Università degli Studi di Milano Bicocca, Piazza della Scienza 4, 20126 Milano, Italy

[*] Corresponding author: Tel.: +86 28 8540 6701 E-mail: zhaotao@scu.edu.cn

Highlights

1. 3D DEM model was used to analyze the impact induced rock fragmentation.
2. The rock fragmentation intensity depends highly on the impact loading rate.
3. The three parameters generalized extreme value distribution function can describe the fragment size distribution characteristics.

Abstract

Rock fragmentation can occur in rapid rock mass movements due to extremely rapid loadings. In this process, the rock block can disintegrate partially or completely depending on the impact loading rate. This contribution presents the results of a series of numerical simulations by the Discrete Element Method (DEM) on the fragmentation of single spherical rock block impact against rigid ground floor, aiming to clarify the fragmentation characteristics. In the analyses, the properties of rock impacting fragmentation are illustrated, regarding the fragment characteristics, the damage ratio, and fragment size distribution pattern. Specific attention is given to the effect of impact loading rate on the fragmentation characteristics. As the loading rate increases, the rock fragmentation intensity increases linearly, while the mean fragment size decreases gradually. In addition, the fragment number exhibits a power law dependence on the loading rate which is in agreement with experimental observations. The measured fragment size distribution can be characterized properly by the three parameters generalized extreme value distribution function, which shows better accuracy than the Weibull distribution function.

Keywords: rock fragmentation; discrete element method; impact loading rate; fragment size distribution; damage ratio

1. Introduction

Rockfalls involving abrupt movements of rock masses detached from steep slopes or cliffs [1] are widely observed in mountainous areas. These events can cause significant hazards to human lives and lifeline facilities [2, 3]. Among various types of block motion (e.g. freefall, bouncing, and rolling), bouncing (impact) is the most complex, uncertain, and poorly understood one [4, 5]. During impacting, the kinetic energy dissipates and the direction of motion changes. Depending on the mechanical properties of the terrain and the rock block, the impact angle, and the block shape, mass, and velocity, the impact process can vary from the elastic to plastic [5, 6]. In addition, during impact, the rock block tends to break, this is especially true for weak rocks [4]. After fragmentation, the motion trajectories of rock fragments are very difficult to predict, increasing the probability of damage to human lives and properties [7]. In this process, the position and the extent of the accumulation zone are strongly affected by rock fragmentation. This phenomenon has been observed by Crosta et al. [8], and they concluded that rock fragmentation influences the runout extent and trajectory of rockfall.

Several parameters can influence the fragmentation process [9, 10], namely, the pre-existing discontinuities, the ground conditions, the impact energy and the impact angle. Through DEM analyses and lab tests, Moreno et al. [11], Samimi et al. [12] and Thornton et al. [13] investigated the granular agglomerate impact fragmentation, and they conclude that the breakage extent of agglomerate mainly depends on the normal component of the impact velocity. Wang and Tonon [9] analysed the effect of impact angle on the rock fragmentation using DEM, and the results indicate that the magnitude of the normal velocity is the main factor influencing the rock fragmentation. De Blasio and Crosta [14] point out that the major fragmentation occurs due to the effect of normal stress acting on the impacting plane rather than the shear stresses. Consequently, it can be concluded that the normal component of the impact velocity plays an important role in rock fragmentation.

Using the open source DEM code ESyS-Particle [15, 16], this paper presents a model of the normal impact induced fragmentation of a synthetic rock under different impact loading rates. The fragmentation characteristics are analysed, including the fragmentation process, the fragmentation intensity, the fragment number, and the fragment size distribution.

2. Model configuration and parameter calibration

In this study, the impact of a rock block with a rigid ground is analysed to investigate the fragmentation characteristics. The numerical model configuration is shown in Fig. 1. In the DEM model, the spherical rock block is represented as an assembly of densely packed and bonded spherical particles. The block has a diameter (D) of 10 cm. It consists of 48,987 randomly distributed spherical particles with the average radius of 1.5 mm, and the ratio of the largest to smallest radius is set as 3. The rigid ground is represented by a layer of fixed particles with a radius of 0.75 mm.

In the rock block, the adjacent particles are bonded together by a bonded particle model (BPM). The bond breakage criterion is introduced according to Wang and Mora [17]. After the bond breaks, the particles will experience cohesionless frictional interaction (CFI) if they come into contact with each other. The interaction model between the rock block and rigid ground is of CFI type as well. A more detailed discussion of the BPM and CFI models can be found in the work of Wang and Mora [17].

To calibrate the DEM model, a series of numerical uniaxial compression tests have been conducted, and the results have been compared with the experimental data on coal rock reported by Liu et al. [18]. The coal rock is chosen for its low strength and brittle nature, and availability of dynamic test data. In the calibration, the DEM parameters are selected by trial and error, and the final values are listed in Table 1. Fig. 2(a) shows the comparison between experimental and numerical stress-strain curves of rock samples under uniaxial compression tests. The numerical stress-strain curves match well the experimental ones, indicating the DEM model can reproduce the mechanical and deformation features of real coal rock. The numerical uniaxial compression tests with different strain rates are performed to investigate the effect of strain-rate on the mechanical responses of specimen. It can be observed that before failure, the stress-strain curves are the same for tests with different strain rates, which match the experimental data well before failure (e.g. $\varepsilon = 0.62\%$) (see Fig. 2(a)). In addition, the strain rate has a minor influence on the peak strength of coal rock. Thus, the current uni-axial compression test can be considered slow enough as quasi-static state, and the obtained peak strength and Young's modulus are identical for the coal rock.

The numerical Split-Hopkinson Pressure Bar (SHPB) tests conducted by Xu et al. [19] and Wang and Tonon [20] are available to investigate the dynamic mechanical response of the synthetic coal rock. The DEM model configuration of the SHPB platform is similar to that described in Xu et al. [19]. The results are compared with the experimental SHPB tests reported by Liu et al. [18]. As shown in Fig. 2(b), the peak compression strength increases with the strain rate, and the elastic modulus remains constant, which are in line with the experimental results.

3. Results

In the analyses, the impact loading rate ($\dot{\varepsilon}$) is defined as v_0/D, with v_0 being the initial impact velocity, D being the diameter of the rock block. The ranges of initial impact velocity and the corresponding loading rates examined in the numerical model are listed in Table 2.

Fig. 3 shows the time evolutions of the fragment number, normalized kinetic energy, E_k, and the damage ratio, α_b, for the impact loading rate of 500 s^{-1}. The normalized kinetic energy is the ratio of the total kinetic energy of the fragments to the initial kinetic energy. The damage ratio, or bond breakage ratio (α_b) [21], which is defined as the ratio of the number of broken bonds to the initial number of bonds, has been used to quantify the rock fragmentation intensity. As shown in Fig. 3, once the rock block impacts upon the ground, the damage ratio and the fragment number increase sharply to the peak values at 100T, and the kinetic energy decreases gradually. The subsequent sliding and collision of fragments also lead to further decrease of kinetic energy, while the damage ratio remain almost unchanged. The slight decrease of fragment number during 100T to 200T is due to the disaggregation of relatively small fragments (e.g. around 10 particle block), leading to fragments smaller than our statistical criterion. In addition, as shown in Fig. 4, the radial displacement of the fragments is very small at 100T, however the displacement increases gradually after 100T and the fragments are ejected. This indicates that the rock fragmentation occurs before fragment ejection, and the fragments ejected by the impacting energy of fragmentation.

Fig. 5 shows the time evolution of the rock block border impacting at different loading rates from a top view. The border is approximated as the connection of the centers of the outermost fragments. As shown in Fig. 5, for the range of tested impact loading rates, the radial displacement is almost nil before 100T, and the fragments were ejected out after 100T.

Fig. 6 shows the plan view of rock fragments after impact for different impact loading rates. According to the plots, it can be observed that as the loading rate increases, the number of fragments and the damage ratio increase, while the average size of fragments decreases with the loading rate. Fig. 7 shows the dependence of the damage ratio (α_b) and fragment number (N) on the impact loading rate. It is clear that the damage ratio increases linearly with the impact loading rate, which is in accordance with the numerical results reported by Thornton et al. [13] and Kafui and Thornton [22]. In addition, the general increasing trend of the fragment number is similar as the experimental data on aluminum rings reported by Grady and Kipp [23], even though the testing method and material are different.

To obtain the fragment size distribution, we defined the characteristic fragment size as

$$d = \sqrt[3]{V_f / V_0} \tag{1}$$

where V_f is the volume of the fragment, and V_0 is the volume of the rock block before impact.

With regard to the fragment size distribution, various distribution functions have been used in the literature [25-27], among which, the Weibull distribution has been widely quoted [28-30]. The Weibull distribution can be expressed as

$$F\left(d;d_c,k\right)=1-\exp\left[-\left(\frac{d}{d_c}\right)^k\right] \quad (2)$$

where d_c and k are fitting parameters.

Hogan et al. [31] proposed a three parameter generalized extreme value distribution to describe the fragment sizes, and it turns out that this distribution function can better fit the experimental data than the Weibull distribution [32]. The generalized extreme value distribution is given by

$$F\left(d;\mu,\sigma,\xi\right)=\exp\left\{-\left[1+\xi(\frac{d-\mu}{\sigma})\right]^{-1/\xi}\right\} \quad (3)$$

where μ is the location parameter, σ is the scale parameter and ξ is the shape parameter.

To compare the aforementioned two distribution relations, the two functions are used respectively to fit the fragment size distribution as weighted by fragment number mass (see Fig. 8 and Fig. 9, respectively). Fig. 8 shows the numerical results and the fitted cumulative frequency distribution. It is obvious that the number based ("Num-based" in the plots) cumulative frequency distribution is in line with the generalized extreme value distribution. As shown in the partial enlargement drawing in Fig. 8 (a) and (b), a large mismatching error exhibits between the Weibull distribution and the numerical results. On the contrary, the generalized extreme value distribution can fit the numerical results with good accuracy. Fig. 9 shows the numerical results and the fitted cumulative mass fraction distribution. Similarly, the generalized extreme value distribution fits the data with a higher accuracy than Weibull distribution.

In the generalized extreme value distribution, two parameters, μ and σ, are important, because μ is determined by the average size of the rock fragments, and σ determines the range of the fragment size distribution. Hence, an investigation of the two parameters can give a further insight into the effect of loading rate on the fragment size distribution. Fig. 10 shows the effect of the impact loading rate on the two fitting parameters. For fragment size distribution weighted by fragment number (Fig. 8(a)), the impact loading rate has a little influence on the two parameters.

For fragment size distribution weighted by fragment mass (Fig. 9(a)), the two parameters decrease gradually with the impact loading rate (see Fig. 10(b)). This means that the fragment size becomes smaller, and the corresponding fragment size distribution becomes narrower as the impact loading rate increases. This phenomenon is as expected, since the increased rock fragmentation intensity and fragment number at high loading rates would lead to reduced fragment size [23].

4. Conclusions

The current numerical study on the impact induced coal rock fragmentation shows that the DEM model allows a qualitatively good simulation of rock block fragmentation. The loading rate has a significant influence on the rock fragmentation behavior. The obtained numerical results indicate that the fragmentation process occurs before fragment ejection, and the ejection motion occurs shortly after the rock disaggregation. In addition, rock samples tested at high impact loading rates would cause much higher fragmentation intensity, and correspondingly, a large amount of smaller fragments, when compared with those tested at low loading rates. The damage ratio increases linearly with the loading rate, and the fragment number exhibits power law dependence on the loading rate, which is in agreement with experimental observations. The size distribution of the resultant fragments can be properly fitted by the three parameters generalized extreme value distribution function than do the Weibull distribution.

Acknowledgements

The data are available upon request from the authors. This research was supported by the National Natural Science Foundation of China (Grant No. 41602289), the State Key Program of National Natural Science of China (Grant No. 51639007), the opening fund of Key Laboratory of Geotechnical and Underground Engineering (Tongji University), Ministry of Education (KLE-TJGE-B1503).

REFERENCE

1. Cruden DM, Varnes DJ. Landslide Types and Processes. *Special Report - National Research Council, Transportation Research Board.* 1958;247: 20-47.
2. Bunce CM, Cruden DM, Morgenstern NR. Assessment of the hazard from rock fall on a highway. *Canadian Geotechnical Journal.* 1997;34(3): 344-356.
3. Chau KT, Wong RHC, Liu J, Lee CF. Rockfall Hazard Analysis for Hong Kong Based on Rockfall Inventory. *Rock Mech Rock Eng.* 2003;36(5): 383-408.
4. Bozzolo D, Pamini R. Simulation of rock falls down a valley side. *Acta Mechanica.* 1986;63(1): 113-130.
5. Azzoni A, Freitas MHD. Experimentally gained parameters, decisive for rock fall analysis. *Rock Mech Rock Eng.* 1995;28(2): 111-124.
6. Chau KT, Wong RHC, Wu JJ. Coefficient of restitution and rotational motions of rockfall impacts. *Int J Rock Mech Min Sci.* 2002;39(1): 69-77.
7. Wang Y. Three-dimensional rock-fall analysis with impact fragmentation and fly-rock modeling. Ph.D. thesis. University of Texas at Austin; 2009.
8. Crosta GB, Agliardi F, Frattini P, Lari S. Key Issues in Rock Fall Modeling, Hazard and Risk Assessment for Rockfall Protection. In: Lollino G, Giordan D, Crosta GB, et al., eds. *Engineering Geology for Society and Territory - Volume 2: Landslide Processes.* Cham: Springer International Publishing; 2015:43-58.
9. Wang Y, Tonon F. Discrete Element Modeling of Rock Fragmentation upon Impact in Rock Fall Analysis. *Rock Mech Rock Eng.* 2010;44(1): 23-35.
10. Dussauge C, Grasso J, Helmstetter A. Statistical analysis of rockfall volume distributions: Implications for rockfall dynamics. *J Geophys Res.* 2003;108(B6): 2286.
11. Moreno R, Ghadiri M, Antony SJ. Effect of the impact angle on the breakage of agglomerates: a numerical study using DEM. *Powder Technol.* 2003;130(1): 132-137.
12. Samimi A, Moreno R, Ghadiri M. Analysis of impact damage of agglomerates: effect of impact angle. *Powder Technology.* 2004;143–144: 97-109.
13. Thornton C, Ciomocos M, Adams M. Numerical simulations of agglomerate impact breakage. *Powder Technol.* 1999;105(1): 74-82.
14. De Blasio FV, Crosta GB. Fragmentation and boosting of rock falls and rock avalanches. *Geophys Res Lett.* 2015;42(20): 8463-8470.
15. Abe S, Place D, Mora P. A Parallel Implementation of the Lattice Solid Model for the Simulation of Rock Mechanics and Earthquake Dynamics. *Pure appl geophys.* 2004;161(11-12): 2265-2277.
16. Utili S, Zhao T, Houlsby GT. 3D DEM investigation of granular column collapse : evaluation of debris motion and its destructive power. *Eng Geol.* 2015;186: 3-16.
17. Wang Y, Mora P. The ESyS_Particle: A New 3-D Discrete Element Model with Single Particle Rotation. *Advances in Geocomputing.* Berlin, Heidelberg: Springer Berlin Heidelberg; 2009:183-228.
18. Liu X, Dai F, Zhang R, Liu J. Static and dynamic uniaxial compression tests on coal rock considering the bedding directivity. *Environ Earth Sci.* 2015;73(10): 5933-5949.
19. Xu Y, Dai F, Xu NW, Zhao T. Numerical Investigation of Dynamic Rock Fracture

Toughness Determination Using a Semi-Circular Bend Specimen in Split Hopkinson Pressure Bar Testing. *Rock Mech Rock Eng.* 2015;49(3): 731-745.

20. Wang Y, Tonon F. Dynamic validation of a discrete element code in modeling rock fragmentation. *Int J Rock Mech Min Sci.* 2011;48(4): 535-545.
21. Thornton C, Yin KK, Adams MJ. Numerical simulation of the impact fracture and fragmentation of agglomerates. *J Phys D: Appl Phys.* 1996;29(2): 424.
22. Kafui K, Thornton C. Numerical simulations of impact breakage of a spherical crystalline agglomerate. *Powder Technol.* 2000;109(1): 113-132.
23. Grady DE, Kipp ME. Mechanisms of dynamic fragmentation: Factors governing fragment size. *Mech Mater.* 1985;4: 311-320.
24. Grady DE, Kipp ME. Mechanisms of dynamic fragmentation: Factors governing fragment size. *Mechanics of Materials.* 1985;4(3): 311-320.
25. Epstein B. The mathematical description of certain breakage mechanisms leading to the logarithmico-normal distribution. *J Franklin Inst.* 1947;244(6): 471-477.
26. Rosin P, Rammler E. The Laws Governing the Fineness of Powdered Coal. *Jinstfuel.* 1933;7: 29-36.
27. Mott NF, Linfoot EH. *A Theory of Fragmentation*: Springer Berlin Heidelberg; 2006.
28. Weibull W. A Statistical Distribution Function of Wide Applicability. *J Appl Mech.* 1951;13(2): 293-297.
29. Carmona HA, Wittel FK, Kun F, Herrmann HJ. Fragmentation processes in impact of spheres. *Phys Rev E: Stat Nonlinear Soft Matter Phys.* 2007;77: 51302.
30. Cheong YS, Reynolds GK, Salman AD, Hounslow MJ. Modelling fragment size distribution using two-parameter Weibull equation. *Int J Miner Process.* 2004;74, Supplement(50): S227-S237.
31. Hogan JD, Rogers RJ, Spray JG, Boonsue S. Dynamic fragmentation of granite for impact energies of 6–28 J. *Eng Fract Mech.* 2011;79: 103-125.
32. Hou T, Xu Q, Yang X, Lu P, Zhou J. Experimental study of the fragmentation characteristics of brittle rocks by the effect of a freefall round hammer. *Int J Fract.* 2015;194(2): 169-185.

Captions

Fig. 1. Configuration of the three-dimensional DEM model. The rock block is spherical (colors indicate different particle radius). The rigid ground is represented by a layer of fixed particles.

Fig. 2. DEM and experimental (Exp.) results of (a) 3D unconfined uniaxial compression tests, and (b) Split-Hopkinson Pressure Bar (SHPB) tests of coal rock. “r” stands for the strain rate used in the compression simulations.

Fig. 3. Time evolutions of fragment number, normalized kinetic energy, E_k, and damage ratio, α_b ($\dot{\varepsilon}$=500 s^{-1}) (the statistics only considers the fragments consisting of more than 10 particles).

Fig. **4.** Impacting fragmentation process of the rock block ($\dot{\varepsilon}$= 500 s^{-1}). For visualization purpose, fragments are colored with a set of distinct colors, while the fragments consisting of less than 10 particles are ignored. “T” is unit time used in the simulation, $T = 5\times10^{-6}$ s.

Fig. 5. Time evolution of the rock block profile impacting at different loading rates from a top view (see also Fig. 6).

Fig. 6. Top view of rock fragments after impact for different impact loading rates. Distinct colors are set to different fragments, and fragments consisting of less than 10 particles are not plot.

Fig. 7. (a) Damage ratio (α_b), (b) Fragment number (N) dependence on the impact loading rate. The inset plot in (a) shows the numerical data of Thornton et al. [13] and Kafui and Thornton [22], while the inset plot in (b) shows the experimental data of aluminum rings reported in Grady and Kipp [24].

Fig. 8. Numerical results (scattered data points) and fitted cumulative frequency distributions (solid lines) of fragments for different impact loading rates using (a) the generalized extreme value distribution, and (b) the Weibull distribution

Fig. 9. Fragment size distribution weighted by mass for different loading rates. Scatters are numerical results, and solid lines are fitted distributions using (a) the generalized extreme value distribution (b) Weibull distribution.

Fig. 10. Fitting parameters of the fragment size distribution weighted by (a) fragment number (b) fragment mass for different impact loading rates

Table 1. Microscopic parameters used in DEM models

Table 2. Range of initial impact velocity and impact loading rate used in the tests.

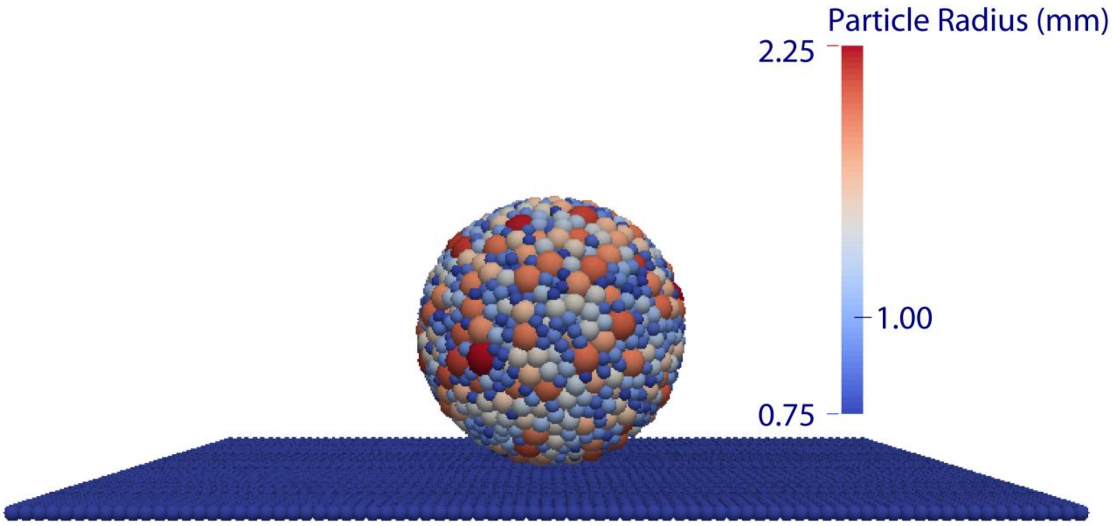

Fig. 1. Configuration of the three dimensional DEM model. The rock block is spherical (colors indicate different particle radius). The rigid ground is represented by a layer of fixed particles.

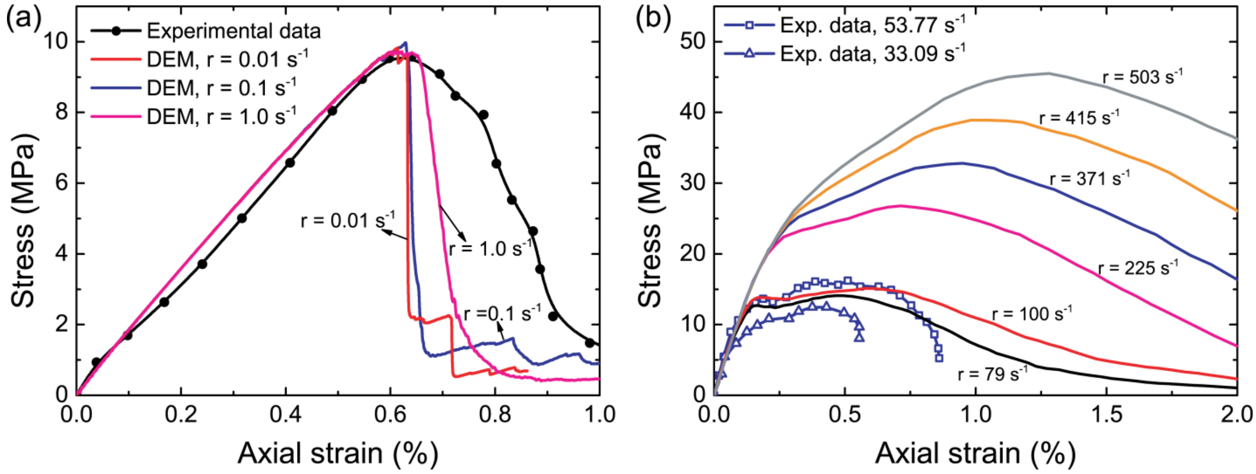

Fig. 2. DEM and experimental (Exp.) results of (a) 3D unconfined uniaxial compression tests, and (b) Split-Hopkinson Pressure Bar (SHPB) tests of coal rock. “r” stands for the strain rate used in the compression simulations.

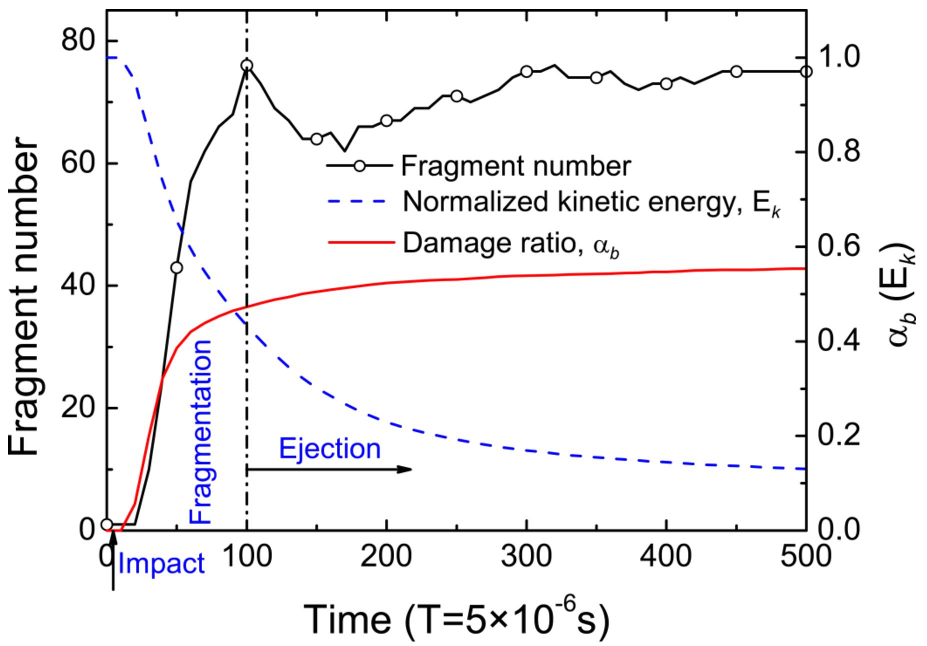

Fig. 3. Time evolutions of fragment number, normalized kinetic energy, E_k, and damage ratio, α_b ($\dot{\varepsilon}$=500 s^{-1}) (the statistics only considers the fragments consisting of more than 10 particles).

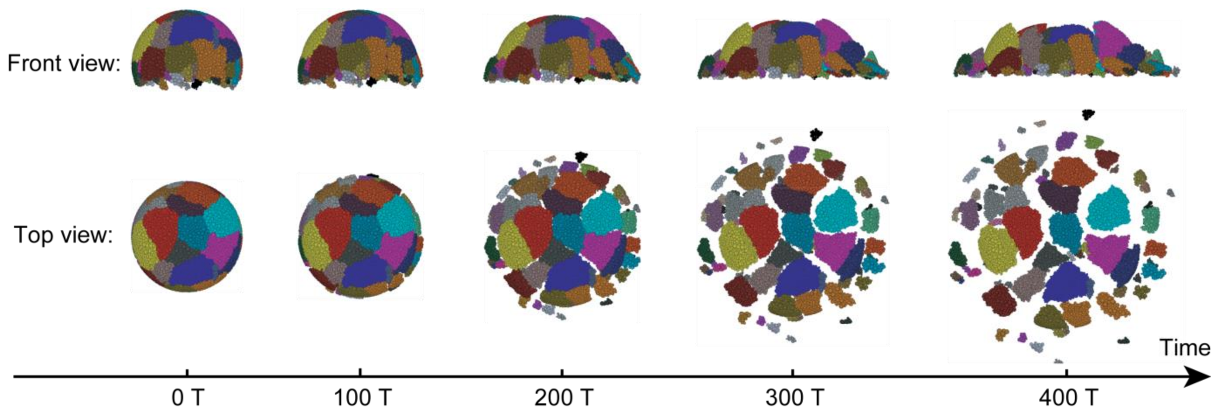

Fig. 4**.** Impacting fragmentation process of the rock block ($\dot{\varepsilon}$= 500 s^{-1}). For visualization purpose, fragments are colored with a set of distinct colors, while the fragments consisting of less than 10 particles are ignored. “T” is unit time used in the simulation, T = 5×10^{-6} s.

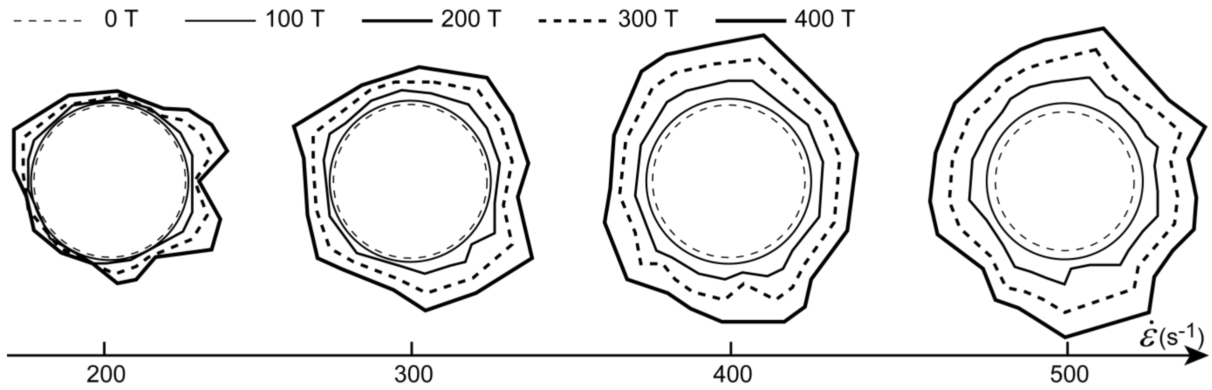

Fig. 5. Time evolution of the rock block profile impacting at different loading rates from a top view (see also Fig. 6).

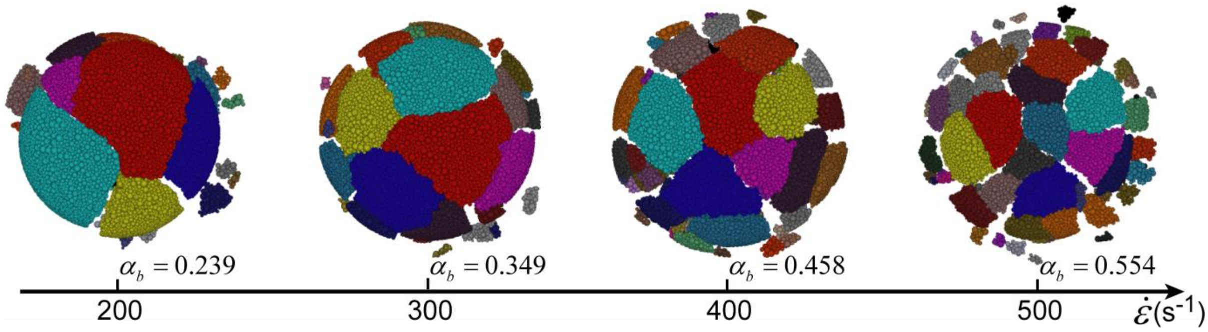

Fig. 6. Top view of rock fragments after impact for different impact loading rates. Distinct colors are set to different fragments, and fragments consisting of less than 10 particles are not plot.

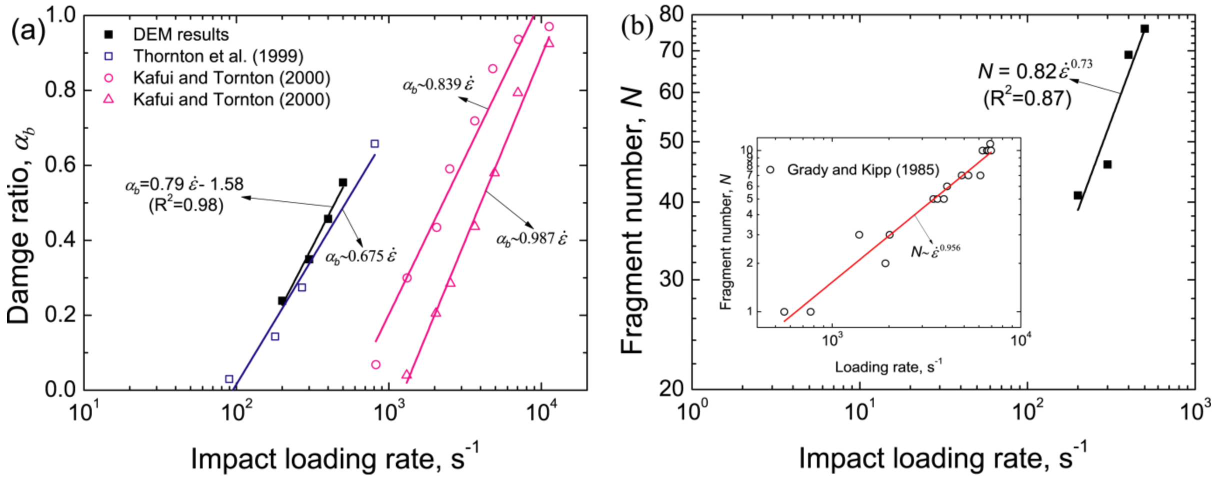

Fig. 7. (a) Damage ratio (α_b), (b) Fragment number (N) dependence on the impact loading rate. The inset plot in (a) shows the numerical data of Thornton et al. [13] and Kafui and Thornton [22], while the inset plot in (b) shows the experimental data of aluminum rings reported in Grady and Kipp [24].

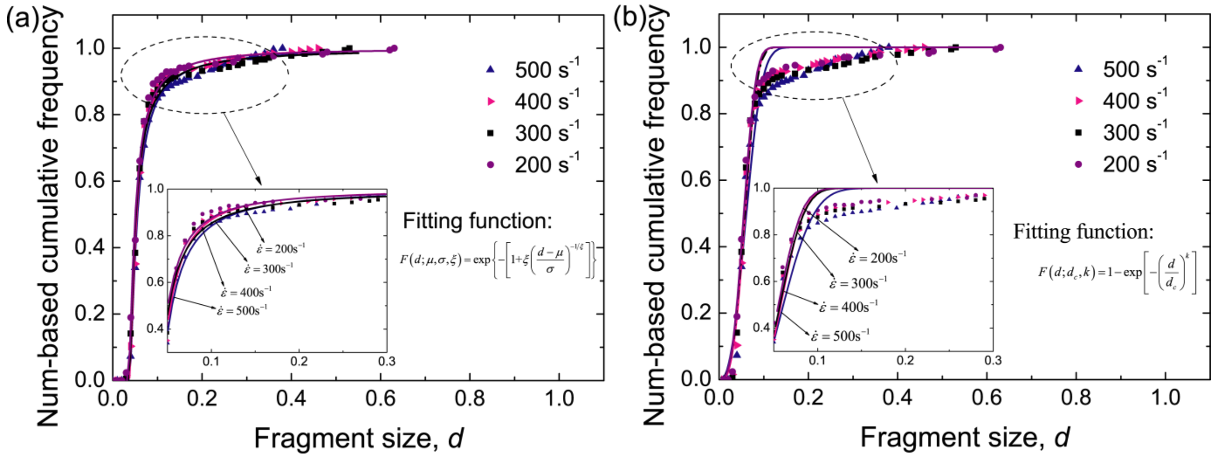

Fig. 8. Numerical results (scattered data points) and fitted cumulative frequency distributions (solid lines) of fragments for different impact loading rates using (a) the generalized extreme value distribution, and (b) the Weibull distribution

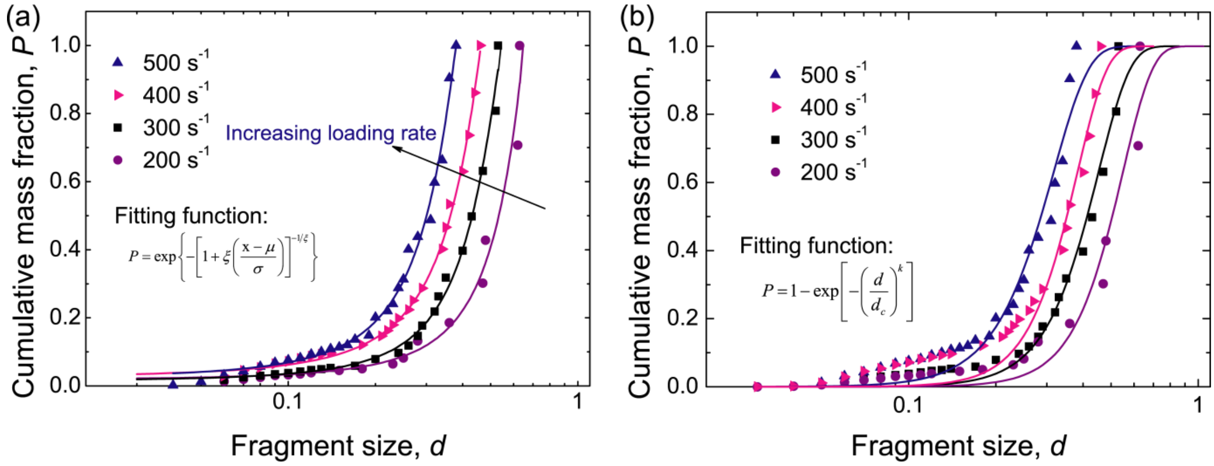

Fig. 9. Fragment size distribution weighted by mass for different loading rates. Scatters are numerical results, and solid lines are fitted distributions using (a) the generalized extreme value distribution (b) Weibull distribution.

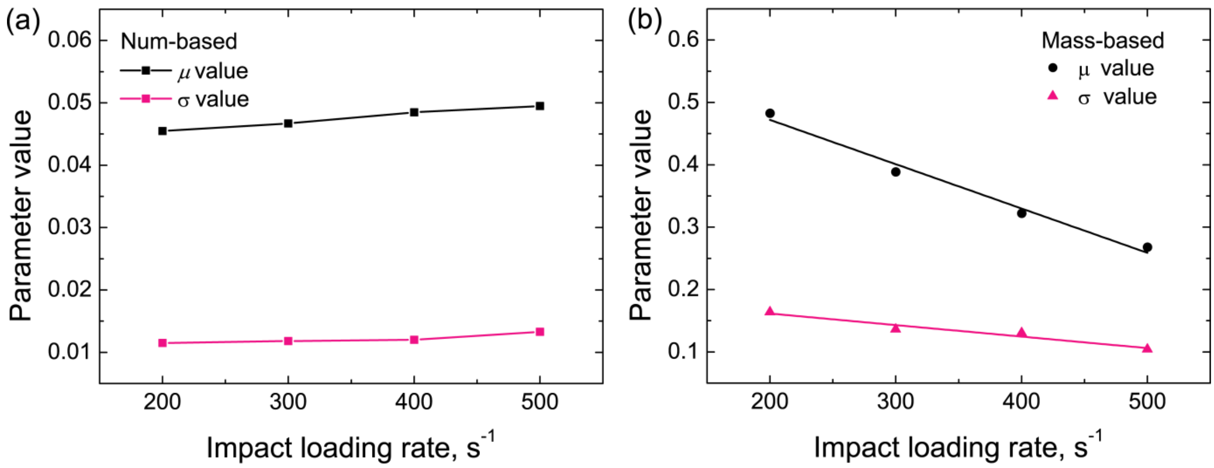

Fig. 10. Fitting parameters of the fragment size distribution weighted by (a) fragment number (b) fragment mass for different impact loading rates

Table 1. Microscopic parameters used in DEM models

Microscopic parameters	
Particle	
Radius (mm)	0.75-2.25
Density (kg/m^3)	2650
Young's modulus (MPa)	5×10^3
Poisson's ratio	0.25
Friction coefficient	0.58
Bond	
Cohesion (MPa)	14.25
Young's modulus (MPa)	1.25×10^3
Friction angle (°)	45
Poisson's ratio	0.25

Table 2. Range of initial impact velocity and impact loading rate used in the tests.

v_0 (m/s)	20	30	40	50
$\dot{\varepsilon}$ (s^{-1})	200	300	400	500